SUPPORTING INFORMATION FOR:

Towards Huygens' Sources with dodecahedral plasmonic clusters

Laurent Lermusiaux,[1,†] Véronique Many,[1,2] Philippe Barois,[2] Virginie Ponsinet,[2] Serge Ravaine,[2] Etienne Duguet,[1] Mona Tréguer-Delapierre[1,] and Alexandre Baron,[2,*]*

[1]Univ. Bordeaux, CNRS, ICMCB, Bordeaux INP, UMR 5026, Pessac 33600, France

[2] Univ. Bordeaux, CNRS, CRPP, UMR 5031, Pessac 33600, France

1) Materials and methods

Materials

Ammonium hydroxide (28.0% to 30.0%, J. T. Baker), sodium hydroxide (NaOH, Sigma-Aldrich, 98%), formaldehyde (ACS reagent, 37 wt. % in water, contains 10-15% methanol as stabilizer, Sigma-Aldrich), gold (III) chloride trihydrate ($HAuCl_4.3H_2O$, Sigma-Aldrich, 99.9%), silver nitrate ($AgNO_3$, Sigma-Aldrich, ≥99.0%), poly(vinylpyrrolidone) (PVP mass average molecular weight 40,000, Merck) and tetrakis(hydroxymethyl)phosphonium chloride (THPC, Aldrich, 80%) were used as received.

Ag dodecapod synthesis

Synthesis of silica particles with 12 functionalized dimples. We first synthesized a silica template with 12 dimples, according to a protocol described in details elsewhere.[1] The sample was characterized by TEM and we determined statistically that it consists of dodecahedral with a morphology yield of 70%. Other side products are silica particles with 8 dimples (6%), 9 dimples (7%), 10 dimples (7%) and mutisilica particles (10%). The final particle concentration in the synthesis was 1.8 10^{12} particles/mL and particles were suspended in water.

Synthesis of gold seeds.[2] Water (227.5 mL) was mixed with 0.2 M NaOH (7.5 mL) and 5 mL of diluted THPC (120 µL of the stock solution diluted in 10 mL of water) for 15 min. Then, 5 mL of $HAuCl_4$ (25 mM) was quickly added and the solution changed from colourless to brown immediately, indicating the formation of gold seeds. This as-prepared gold-seed solution was kept at 4°C at least 14 days before use. Gold seeds are 2-3 nm in diameter.

Decoration of the dimples with gold seeds. Aminated silica particles (10 mL corresponding to 1.8 10^{13} particles) were mixed with the gold seeds solution (30 mL). The reaction medium was

stirred overnight on a roller mixer. The dispersion was washed twice by centrifugation (8000g for 10 min) to remove the free gold seeds, and was redispersed in a PVP solution (40 mL, 1g/L).

Growth of the Au seeds into Ag pods. Silica particles (50 µL of the previous solution) were diluted in a volume of MilliQ water calculated to obtain a final volume of 10 mL after addition of all the reactants. To the silica particle solution were consecutively added, under vigorous stirring, 30 mM silver nitrate (see Table S1 for volumes), formaldehyde (10 µL) and diluted ammonium hydroxide (200 µL dropwise, 1/100 dilution). The dropwise rate was roughly 10 µL of solution every 3 seconds. The initial light pink color changes drastically upon addition of the ammonium hydroxide (see Figure S1). The sample was centrifuged 2 minutes after the end of the reactant addition (10 min, from 6000g to 2000g with increasing satellite size) and redispersed in 10 ml of MilliQ water.

Table S1. Silver quantity used for the preparation of the different samples and the corresponding silver satellite radius. The radius was statistically measured for A_6 (Fig S3) on TEM images and estimated for other samples knowing the quantity of silver used.

Sample	A_1	A_2	A_3	A_4	A_5	A_6	A_7	A_8	A_9	A_{10}	A_{11}	A_{12}
V($AgNO_3$) 30 mM (in µL)	6	9	13.5	20.3	30.4	45.6	68.3	102.5	153.8	230.7	346	519
Estimated satellite radius (in nm)	13.9	16	18.3	20.9	24	27.4	31.4	35.9	41.1	47	53.9	61.2

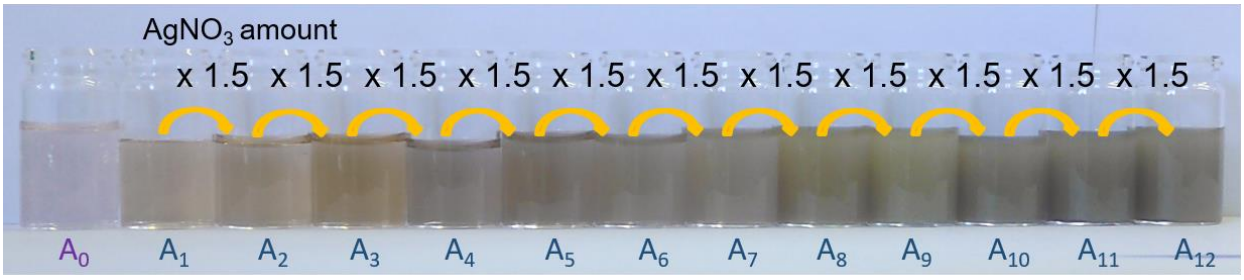

Figure S1. Picture of the gold-seeded sample (A_0) and the 12 Ag dodecapods batches with increasing Ag satellite sizes (A_1 to A_{12}).

2) Electron microscopy

Electron microscopy characterization

Scanning transmission electron microscopy (STEM) studies were performed using a JEOL cold-FEG JEM-ARM200F operated at 200kV equipped with a probe Cs corrector reaching a spatial resolution of 0.078 nm. EDX spectra were recorded on a JEOL CENTURIO SDD detector. TEM experiments were performed using a JEOL JEM 1400+ at 120 kV with a LaB6 filament. We prepared the samples by depositing one drop of the colloidal dispersion on a conventional carbon-coated copper grid. We then air-dried the grids at room temperature and stored them in a close box to prevent dust accumulation. SEM experiments were performed on a JEOL 6700F.

Additional electron microscopy images

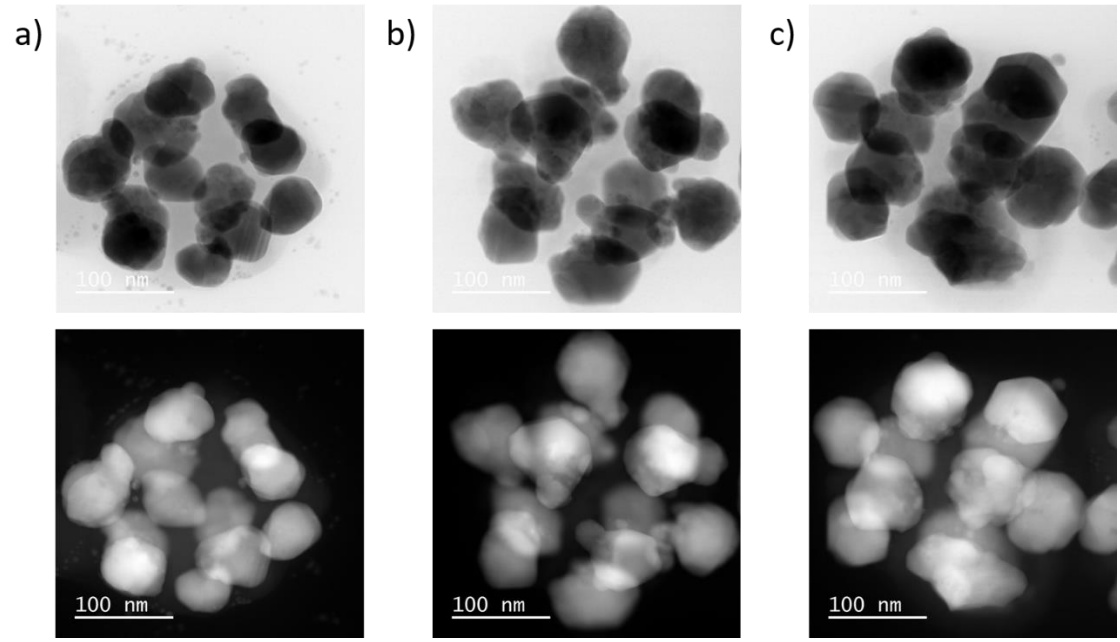

Figure S2. Bright-field (top images) and high-angle annular dark-field (HAADF) (bottom images) STEM close-ups of silver dodecapods from samples (a) A_6 (b) A_8 and (c) A_{10}

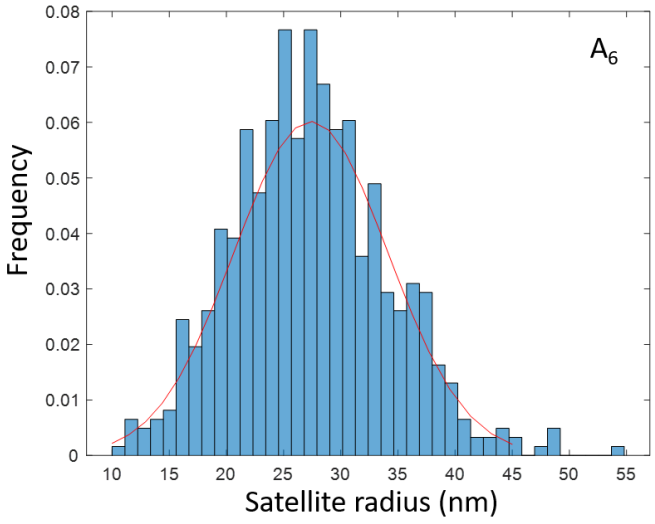

Figure S3. Histogram of the experimental distribution of silver satellites measured for sample A_6. The red line is the fitted normal distribution used to compute the scattering properties in the case of polydisperse systems.

3) Optical characterization

UV-Vis spectroscopy spectra were recorded on a Shimadzu UV-3600 UV-VIS-NIR.

The static light scattering measurements (SLS) were carried out on a homemade optical platform described below and sketched in Figure S4. The light source is a supercontinuum laser SuperK Extreme EXB-6 from NKT Photonics equipped with a filter module KSplit enabling to deliver a white beam spanning the spectral range from 440 to 900 nm. The beam is linearly polarized by a Glan-Taylor polarizer P1 (Thorlabs GL5) and a motorized Half-Wave Fresnel Rhomb Retarder (Thorlabs FR600HM) rotates the polarization at angle φ from the scattering plane. A converging achromatic lens (f= 100mm Thorlabs AC254-100-A-ML) focuses the input beam into the sample cell. The scattered light is collected at angle θ_{Scat} from the direct beam and analyzed by a second polarizer P2 (Thorlabs GL10) set either parallel or perpendicular to the scattering plane. A collimated fiber injects the scattered light into a spectrometer with a 2 nm resolution (Hamamatsu

C10083CA). A motorized goniometer (Brookhaven Instruments) spans the scattering angle range from 20 to 140 degrees. The cylindrical sample cell, made of fused silica ∅ = 10 mm, is filled with the dodecapod suspension and introduced in a conventional cylindrical glass vat filled with an index-matching liquid.

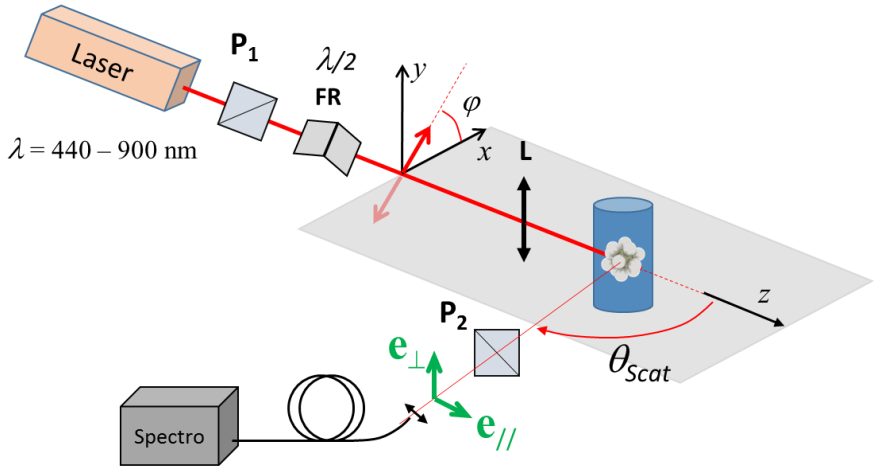

Figure S4. Schematic view of the light scattering setup. The rotation of the input polarization with the half-wave Fresnel rhombohedron controls the incident polarization angle φ. The output polarizer P_2 enables to collect the scattering along the directions perpendicular ($\mathbf{e}_\perp$) and parallel ($\mathbf{e}_{//}$) to the scattering plane shown in grey shade. L is a focusing lens.

Extinction profile

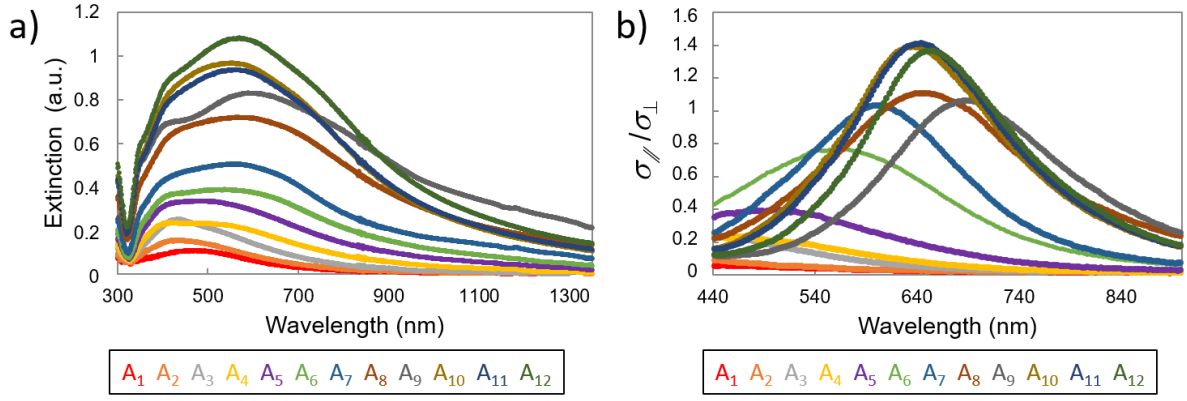

Figure S5. UV-Vis spectra (a) and plot of the experimental function $\sigma_{//}(90°)/\sigma_{\perp}(90°)$ as an estimator of the ratio of the magnetic to electric dipolar scattering (b) for Ag dodecapods with increasing satellite size.

Figure S5 shows a clear resonant behavior with a maximum in the range 450-650 nm. The broad shape of the extinction signal and its evolution from A_3 to A_{10} denotes the presence of at least two scattering features at 420 nm and 520-600 nm, the latter growing and red-shifting with the size of the satellites, hence revealing a strong electromagnetic coupling of the satellites when the size-to-separation ratio increases.

4) Theoretical approach

We use the scattering matrix formalism to write the scattered fields parallel ($E_{Scat/\!/}$) and perpendicular ($E_{Scat\perp}$) to the scattering plane[3] for a single isotropic scatterer:

$$\begin{pmatrix} E_{Scat/\!/} \\ E_{Scat\perp} \end{pmatrix} = \frac{e^{ikr}}{-ikr} \begin{pmatrix} S_2 & 0 \\ 0 & S_1 \end{pmatrix} \begin{pmatrix} E_0 \cos\phi \\ E_0 \sin\phi \end{pmatrix} \qquad \text{Eq-1}$$

Like in the Mie theory, the scattered fields can be expanded in series of vector spherical harmonics and the matrix elements can be expressed as:

$$S_1 = \sum_n \frac{2n+1}{n(n+1)} (a_n^{DDP}\pi_n + b_n^{DDP}\tau_n)$$
$$S_2 = \sum_n \frac{2n+1}{n(n+1)} (a_n^{DDP}\tau_n + b_n^{DDP}\pi_n) \qquad \text{Eq-2}$$

Where the scattering coefficients a_n^{DDP} and b_n^{DDP} have the same meaning as in the Mie theory, namely the electric and magnetic response of the n^{th} multipole, but with different values that can be given by numerical simulations. The a_n^{DDP} and b_n^{DDP} coefficients depend on the structure of the dodecapods and on the wavelength, whereas the θ dependence is borne by the π_n and τ_n only[3] defined as $\pi_n = -\frac{1}{\sin\theta}\frac{dP_n(\mu)}{d\theta}$ and $\tau_n = -\frac{d^2P_n(\mu)}{d\theta^2}$ where P_n is the Legendre polynomial and $\mu = \cos\theta$.

The experimental scattered intensities recorded along the two output channels then read:

$$I_{Scat\perp}(\lambda,\theta,\phi) = I_0(\lambda)N_{DDP}\frac{|S_1(\theta)|^2}{k^2}\delta\Omega\ g(\lambda,\delta\Omega) \times sin^2\phi = A_\perp(\theta,\lambda)\,sin^2\phi$$
$$I_{Scat/\!/}(\lambda,\theta,\phi) = I_0(\lambda)N_{DDP}\frac{|S_2(\theta)|^2}{k^2}\delta\Omega\ g(\lambda,\delta\Omega) \times cos^2\phi = A_{/\!/}(\theta,\lambda)\,cos^2\phi \quad \text{Eq-3}$$

Where $I_0(\lambda)$ is the irradiance of the light source, N_{DDP} is the number of scatterers in the scattering volume, k is the wavenumber, $\delta\Omega$ is the solid angle and the unknown function $g(\lambda,\delta\Omega)$ accounts for the spectral sensitivity of the detector and the optical transmission or reflection of all optical elements. The scattering data are recorded by scanning the polarization angle φ over a 360° range by 10° steps and the scattering amplitudes $A_\perp$ and $A_{/\!/}$ are extracted by fitting the data to $\sin^2$ and $\cos^2$ functions.

In order to extract the terms of interest $|S_1(\theta)|^2$ and $|S_2(\theta)|^2$, we perform an additional measurement of the scattering from a dilute suspension of calibrated polystyrene nanospheres (∅=104 nm).

$$I^{PS}_{Scat\perp}(\lambda,\theta,\phi) = I_0(\lambda)N_{PS}\frac{|S_1^{PS}(\theta)|^2}{k^2}\delta\Omega\ g(\lambda,\delta\Omega) \times sin^2\phi = A^{PS}_\perp(\lambda)\,sin^2\phi \quad \text{Eq-4}$$

Dividing equations Eq-3 by Eq-4 yields the differential scattering cross-sections of the dodecapods:

$$\sigma_\perp(\theta) = \frac{|S_1(\theta)|^2}{k^2} = \frac{N_{DDP}}{N_{PS}}\frac{A_\perp}{A^{PS}_\perp}\frac{|S_1^{PS}(\theta)|^2}{k^2}$$
$$\sigma_{//}(\theta) = \frac{|S_2(\theta)|^2}{k^2} = \frac{N_{DDP}}{N_{PS}}\frac{A_{/\!/}}{A^{PS}_\perp}\frac{|S_1^{PS}(\theta)|^2}{k^2} \quad \text{Eq-5}$$

The ratios $A_\perp/A^{PS}_\perp$ and $A_{/\!/}/A^{PS}_\perp$ come out from the experimental data and $|S_1^{PS}(\theta)|^2$ is simply calculated from the Mie theory for a polystyrene sphere. Since the ratio of concentrations is not known within a reasonable accuracy, the differential cross-sections are only known within a constant scaling factor.

The scattering angle $\theta = 90°$ plays a special role since the $\pi_n(\pi/2)$ and $\tau_n(\pi/2)$ are alternatively zero for increasing n :

$$S_1(90°) = \frac{3}{2}a_1^{DDP} + \frac{5}{2}b_2^{DDP} + \frac{7}{8}a_3^{DDP} + \cdots$$
$$S_2(90°) = \frac{3}{2}b_1^{DDP} + \frac{5}{2}a_2^{DDP} + \frac{7}{8}b_3^{DDP} + \cdots \quad \text{Eq-6}$$

Therefore, the differential scattering cross-sections $\sigma_{\perp}(90°)$ and $\sigma_{/\!/}(90°)$ plotted in Figure 3b separate two series of contributions from the electric dipole, magnetic quadrupole, electric octupole, etc... for $\sigma_{\perp}(90°)$ and magnetic dipole, electric quadrupole, magnetic octupole, etc... for $\sigma_{/\!/}(90°)$.

At dipolar order ($n = 1$) which is expected to be dominant at the lowest resonance frequencies, the ratio $\sigma_{/\!/}(90°)/\sigma_{\perp}(90°)$ plotted in Figure 3a measures the strength $|b_1^{DDP}|^2/|a_1^{DDP}|^2$of the magnetic dipole relative to the electric dipole. At shorter wavelengths, when higher order multipoles are excited and may overlap, the signification of the ratio is more complex. The identification of the multipole order of the resonances observed in the experimental data requires the help of numerical simulations.

For scattering angles θ other than 90°, the full series of multipoles contribute to both the parallel and transverse scattering cross-sections. The normalization with the polystyrene reference is still useful and equations 5 are used to draw the polar plots shown in figure 5.

5) Numerical simulations

Multipolar decomposition of the scattering by dodecahedral nanoclusters

Simulations are carried out using the finite-element based software COMSOL Multiphysics. The dodecahedral nanocluster is composed of 13 spheres: a central core sphere and 12 satellite spheres. The entire system is surrounded by perfectly matched layers (PMLs) in order to account for an infinite host medium. The host medium is water and the index of refraction is set to 1.33. The index of the silica core is set to 1.44. The total scattering cross-section is determined by computing

the flux of the Poynting vector average across a close boundary (a sphere) surrounding the nanocluster. The currents generated inside the nanocluster are projected on a vector spherical harmonic basis using Grahn's decomposition.[4] The projections are carried out, up to the third order (octupole) for both electric and magnetic multipoles. This in turn, enables retrieving the scattering cross-section contribution of each multipole.[5] The even (resp. odd) multipole scattering cross-sections is determined by adding the contributions of the electric (resp. magnetic) dipole, magnetic (resp. electric) quadrupole and the electric (resp. magnetic) octupole. To ensure that sufficiently many multipole contributions have been taken into account, the total scattering cross-section computed using the multipolar decompositions is compared to that computed with the average Poynting vector flux method.

The multipolar coefficients are also used to compute $|S_1|^2/k^2$ and $|S_2|^2/k^2$, where S_1 and S_2 are the first and second coefficients of the scattering matrix using Bohren & Huffman's convention.[3]

Definition of the Efficiency for Backscattering

The efficiency for backscattering used in the mains manuscript is defined in section 4.6 of Chapter 4 in C.F. Bohren and D. R. Huffman's famous monograph[3]. It can be used to state the Generalized Kerker condition (GK). Indeed, the GK condition is expressed mathematically as follows

$$GK: K = \sum_{n}^{+\infty} (2n+1)(-1)^n (a_n - b_n) = 0 \qquad \text{Eq-7}$$

K is a complex quantity and whenever it is equal to 0, the backscattering is rigorously suppressed. The efficiency for backscattering which is proportional to the magnitude squared of GK

$$EFB = \frac{|K|^2}{k^2 R^2} \quad \text{Eq-8}$$

where R is the radius of the particle. As a result, the GK condition is equivalent to EFB = 0. The EFB is actually interpreted as the differential scattering cross-section for scattering into a unit solid angle around the backscattering direction, normalized by the geometric cross-section of the sphere (πR^2).

Simulation of polydispersity

To account for polydispersity, simulations of dodecahedral nanoclusters are carried out for varying radii of the silver satellites equally spaced over the [10 nm – 45 nm] range. The experimental distribution is fitted using a normal distribution and the scattering from each simulated nanocluster is weighted using the fitted distribution.

REFERENCES

(1) Many, V.; Dézert, R.; Duguet, E.; Baron, A.; Jangid, V.; Ponsinet, V.; Ravaine, S.; Richetti, P.; Barois, P.; Tréguer-Delapierre, M. High Optical Magnetism of Dodecahedral Plasmonic Meta-Atoms. *Nanophotonics* **2018**, *8* (4), 549–558.

(2) Duff, D. G.; Baiker, A.; Edwards, P. P. A New Hydrosol of Gold Clusters. 1. Formation and Particle Size Variation. *Langmuir* **1993**, *9* (9), 2301–2309.

(3) Bohren, C. F.; Huffman, D. R. *Absorption and Scattering of Light by Small Particles*; John Wiley & Sons, 2008.

(4) Grahn, P.; Shevchenko, A.; Kaivola, M. Electromagnetic Multipole Theory for Optical Nanomaterials. *New J. Phys.* **2012**, *14* (9), 093033.

(5) Dezert, R.; Richetti, P.; Baron, A. Complete Multipolar Description of Reflection and Transmission across a Metasurface for Perfect Absorption of Light. *Opt. Express, OE* **2019**, *27* (19), 26317–26330.